

An anomalous topological phase transition in spatial random graphs

Jasper van der Kolk ^{1,2}, M. Ángeles Serrano ^{1,2,3} & Marián Boguñá ^{1,2}✉

Clustering—the tendency for neighbors of nodes to be connected—quantifies the coupling of a complex network to its latent metric space. In random geometric graphs, clustering undergoes a continuous phase transition, separating a phase with finite clustering from a regime where clustering vanishes in the thermodynamic limit. We prove this geometric to non-geometric phase transition to be topological in nature, with anomalous features such as diverging entropy as well as atypical finite-size scaling behavior of clustering. Moreover, a slow decay of clustering in the non-geometric phase implies that some real networks with relatively high levels of clustering may be better described in this regime.

¹Departament de Física de la Matèria Condensada, Universitat de Barcelona, Martí i Franquès 1, 08028 Barcelona, Spain. ²Universitat de Barcelona Institute of Complex Systems (UBICS), Universitat de Barcelona, Barcelona, Spain. ³ICREA, Pg. Lluís Companys 23, E-08010 Barcelona, Spain. ✉email: marian.boguna@ub.edu

For many years, Landau's theory of symmetry breaking was believed to be the ultimate explanation of continuous phase transitions¹. In the liquid-crystal transition, for instance, the continuous translational and rotational symmetry at high temperatures break into a set of discrete symmetries in the low-temperature phase. This paradigm was challenged by Berezinskii, Kosterlitz, and Thouless (BKT) in the two-dimensional XY model^{2–4}. For this model, the Mermin–Wagner theorem⁵ states that there is no ordered phase even at zero temperature, so that a phase transition in Landau's sense cannot exist. Yet, BKT showed that, in fact, there is a finite temperature phase transition driven by topological defects: vortices and antivortices. At low temperature, vortex-antivortex pairs are bound together. Above the critical temperature, vortex-antivortex pairs unbind, moving freely on the surface. No symmetry is broken in the transition since both phases are rotationally invariant and so magnetization is zero in both phases. Topological order and topological phase transitions are nowadays fundamental to understand the properties of quantum matter⁶.

We study this type of transition in the framework of complex networks, more specifically that of sparse geometric random network models. We use a geometric description of networks⁷ as it provides a simple and comprehensive approach to complex networks. The existence of latent metric spaces underlying complex networks offers a deft explanation for their intricate topologies, giving at the same time important clues on their functionality. The small-world property, high levels of clustering, heterogeneity in the degree distribution, and hierarchical organization are all topological properties observed in real networks that find a simple explanation within the network geometry paradigm⁷. Within this paradigm, the results found in this work hold in a very general class of spatial networks defined in compact homogeneous and isotropic Riemannian manifolds of arbitrary dimensionality^{8–13}. Yet, in this paper, we focus on the \mathbb{S}^1 model⁹ and its isomorphically equivalent formulation in the hyperbolic plane, the \mathbb{H}^2 model¹⁴. Interestingly, many analytic results have been derived for the $\mathbb{S}^1/\mathbb{H}^2$ model, e. g. degree distribution^{9,14,15}, clustering^{14–17}, diameter^{18–20}, percolation^{21,22}, self-similarity⁹, or spectral properties²³ and it has been extended to growing networks²⁴, as well as to weighted networks²⁵, multilayer networks^{26,27}, networks with community structure^{28–30} and it is also the basis for defining a renormalization group for complex networks^{31,32}. The analytical tractability of the \mathbb{S}^1 model makes it the perfect framework for our work.

In this paper, we study a transition taking place in a very general class of sparse spatial random network models and show that it is, in fact, topological in nature. We show that both its thermodynamic properties as well as the finite size scaling behavior are, to the best of our knowledge, novel, and different to those observed in the BKT transition. We structure the paper in the following way: First, we introduce the \mathbb{S}^1 -model, which will be used to obtain both analytical as well as numerical results for the phase transition. Then, by mapping the network model to a model of non-interacting fermions, we are able to study analytically the behavior of the entropy at the critical point, showing that it diverges in the thermodynamic limit at the critical point, unlike in the case of the BKT transition. Next, we prove that the transition is topological in nature by noticing that in the transition, chordless cycles in the network play the role of topological defects with respect to a tree. The critical temperature separates a low-temperature phase, where the underlying metric space forces chordless cycles to be short range –mostly triangles– and a high-temperature phase, where chordless cycles decouple from the metric space and become of the order of the network diameter. This is similar to the unbinding of vortex-antivortex pairs in the

BKT transition. These two distinct topological orders of the transition can be quantified by means of the average local clustering coefficient, a measure of the fraction of triangles attached to nodes. Clustering is finite in the geometric phase with short-range cycles and vanishes in the thermodynamic limit of the non-geometric phase with long-range chordless cycles. Thus, the local average clustering coefficient can be used to study the finite-size scaling behavior of the transition. This geometric to non-geometric phase transition shows interesting atypical scaling behavior as compared with standard continuous phase transitions, where one observes a power law decay at the critical point and a faster decay in the disordered phase. Instead, at the critical point, the average local clustering coefficient decays logarithmically to zero for very large systems and, in the non-geometric phase, where the coefficient decays as a power law, we discover a quasi-geometric region where the exponent that characterizes this decay depends on the temperature.

Results and discussion

The \mathbb{S}^1 -model. In the \mathbb{S}^1 model, nodes are assumed to live in a metric similarity space, where similarity refers to all the attributes that control the connectivity in the network, except for the degrees. At the same time, nodes are heterogeneous, with nodes with different levels of popularity coexisting within the same system. The popularity of a given node is quantified by its hidden degree. In our model, expected degrees can match observed degrees in real networks and we fix the positions of nodes in the metric space so that generated networks can be compared against real networks. This imposes constraints on the connection probability. Specifically, a link between a pair of nodes is created with a probability that resembles a gravity law, increasing with the product of nodes' popularities and decreasing with their distance in the similarity space. We further ask the model to define an ensemble of geometric random graphs with maximum entropy under the constraints of having a fixed expected degree sequence. This determines completely the form of the connection probability depending on the value of one of the model parameters: temperature⁸. Next, we describe the \mathbb{S}^1 model in the low and high-temperature regimes. Further technical details can be found in Supplementary Note 1.1.

The \mathbb{S}^1 is a model with hidden variables representing the location of the nodes in a similarity space and their popularity within the network. Specifically, each node is assigned a random angular coordinate θ_i distributed uniformly in $[0, 2\pi]$, fixing its position in a circle of radius $R = N/2\pi$. In this way, in the limit $N \gg 1$ nodes are distributed in a line according to a Poisson point process of density one with periodic boundary conditions. Each node is also given a hidden degree κ_i , which corresponds to its ensemble expected degree. In the low temperature regime, each pair of nodes is connected with probability

$$P_{ij} = \frac{1}{1 + \left(\frac{x_{ij}}{\hat{\mu}\kappa_i\kappa_j}\right)^\beta}, \quad (1)$$

where $x_{ij} = R\Delta\theta_{ij}$ is the distance between nodes i and j along the circle, and $\beta > \beta_c = 1$ and $\hat{\mu} = \frac{\beta}{2\pi\langle k \rangle} \sin \frac{\pi}{\beta}$ are model parameters fixing the average clustering coefficient (\bar{c}) and average degree ($\langle k \rangle$) of the network, respectively⁸. In this representation, the parameter β plays the role of the inverse temperature, controlling the level of noise in the system.

In the high temperature regime $\beta < \beta_c$ we again fix the angular coordinate and expected degree of the nodes (κ_i, θ_i) so that the degree distribution of the network remains unaltered when temperature is increased beyond the critical point and the model

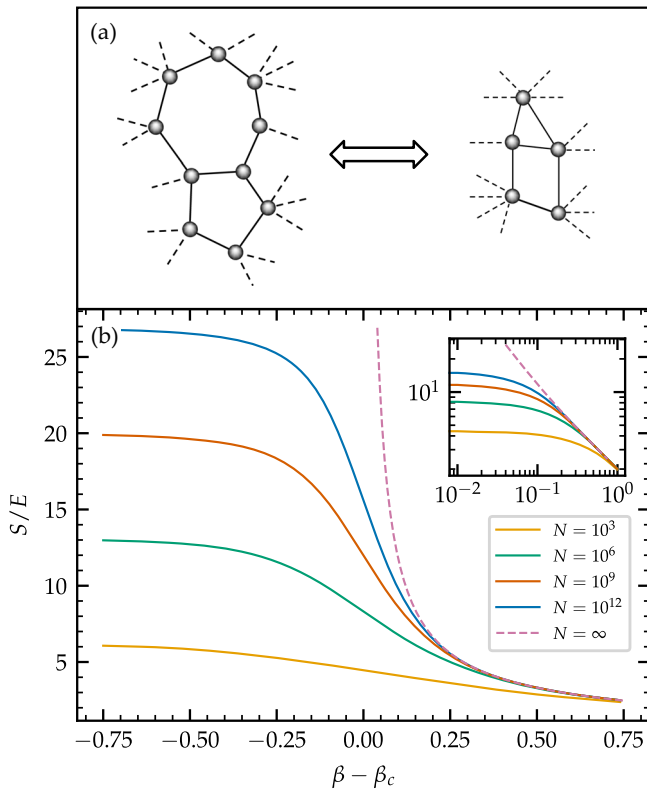


Fig. 1 Behavior of the network model as one crosses the critical temperature, both from an entropic as topological perspective. **a** Sketch illustrating the different organization of cycles in the two phases, short-range at low temperatures and long-range --of the order of the network diameter-- in the high temperature regime. **b** Entropy per link for S^1 geometric networks of different sizes with homogeneous degrees. Different curves are obtained by numerical integration (see Supplementary Note 1.2). The inset shows the same curves in the region $\beta > \beta_c$ in logarithmic scale.

can be directly compared with real networks. Under these constraints, maximizing the entropy of the ensemble leads to the following connection probability⁸

$$P_{ij} = \frac{1}{1 + \frac{x_{ij}^\beta}{\hat{\mu}\kappa_i\kappa_j}}, \tag{2}$$

with $\hat{\mu} \simeq (1 - \beta)2^{-\beta}N^{\beta-1}/\langle k \rangle$ for $\beta < 1$ and $\hat{\mu} \simeq (2\langle k \rangle \ln N)^{-1}$ when $\beta = 1$ (Here we define ‘ $A \simeq B$ ’ as ‘ A is asymptotically equal to B ’, i.e. that the equality becomes exact as $N \rightarrow \infty$. This in contrast to ‘ $A \sim B$ ’ which means that A and B are asymptotically proportional to one another). Notice that this definition of the model converges to the soft configuration model with a given expected degree sequence^{33–36} in the limit of infinite temperature $\beta = 0$. As we show in Supplementary Note 1.2, in this regime long range connections dominate, which causes the entropy density to scale as $\ln N$ (see Fig. 1) in the whole interval $\beta \in [0, 1]$ (and so to diverge in the limit $N \rightarrow \infty$) and the clustering to vanish in the thermodynamic limit.

Entropy and the phase transition. Now that we have defined the model both above and below the critical point $\beta_c = 1$, we can study if the transition in the local properties (the presence of triangles attached to nodes) affects the global behavior of the system (codified by the thermodynamic properties, specifically the entropy). To this end, we show that, for $\beta > \beta_c$, the networks generated by the S^1 -model can be mapped exactly to a gas of identical particles with Fermi statistics. First, we note that the

connection probability in Eq. (1) can be rewritten as the Fermi distribution⁸

$$P_{ij} = \frac{1}{e^{\beta(\epsilon_{ij} - \mu)} + 1}, \tag{3}$$

where the energy of state ij is

$$\epsilon_{ij} = \ln \left[\frac{x_{ij}}{\kappa_i\kappa_j} \right] \tag{4}$$

and where the chemical potential $\mu = \ln \hat{\mu}$ fixes the expected number of links, as in the grand canonical ensemble. Second, links in our model are unlabeled –and so indistinguishable– objects. Third, the model generates simple graphs such that only one link can occupy a given state of energy ϵ_{ij} , which implies that the links respect the Fermi exclusion principle. Finally, such a state is occupied with the probability given in Eq. (3), which is the occupation probability of the Fermi statistics in the grand canonical ensemble. Thus, the S^1 model is equivalent to a system of noninteracting fermions at temperature $T = \frac{1}{\beta}$ ^{8,14}. These Fermi-like “particles” correspond to the links of the network and live on a discrete phase space defined by the $N(N - 1)/2$ pairs among the N nodes of the network. Each such state ij has an associated energy given by ϵ_{ij} , which grows slowly with the distance between nodes i and j in the metric space.

Despite the fact that links in the model are noninteracting particles, the system undergoes a continuous phase transition at a critical temperature $T_c = \beta_c^{-1} = 1$, separating a geometric phase, with a finite fraction of triangles attached to nodes induced by the triangle inequality, and a non-geometric phase, where clustering vanishes in the thermodynamic limit⁹. We can analyze the nature of the transition by studying the entropy of the ensemble. Given the mapping of the S^1 model to a system of non-interacting fermions in the grand canonical ensemble, we start from the grand canonical partition function

$$\ln \mathcal{Z} = \sum_{i < j} \ln \left[1 + \left(\frac{x_{ij}}{\hat{\mu}\kappa_i\kappa_j} \right)^{-\beta} \right], \tag{5}$$

where $\hat{\mu} = \exp \mu$. Given the homogeneity and rotational invariance of the distribution of nodes in the similarity space, we can place the i ’th node on the origin, leading to N identical terms. When the system size is large, we can approximate the sums in Eq. (5) by integrals. This leads to the following expression

$$\begin{aligned} \ln \mathcal{Z} &= N \iint d\kappa d\kappa' \rho(\kappa)\rho(\kappa') \int_0^\infty dx \ln \left[1 + \left(\frac{x}{\hat{\mu}\kappa\kappa'} \right)^{-\beta} \right] \\ &= N\hat{\mu}\langle k \rangle^2 \int_0^\infty dt \ln [1 + t^{-\beta}] = N \frac{\hat{\mu}\langle k \rangle^2 \pi}{\sin \frac{\pi}{\beta}}. \end{aligned} \tag{6}$$

We can then use the above expression to find the grand potential $\Xi = -\beta^{-1} \ln \mathcal{Z}$ and the entropy as $S = \beta^2 \left(\frac{\partial \Xi}{\partial \beta} \right)_\mu$. From this, we can find the entropy per link of the system as

$$\frac{S}{E} = \beta - \pi \cot \frac{\pi}{\beta} \stackrel{\beta \rightarrow \beta_c^+}{\sim} \frac{1}{\beta - 1}, \tag{7}$$

where in the last step $\hat{\mu}$ was plugged in. Note that $E = N\langle k \rangle/2$ is the number of links –and so particles– in the network. Interestingly, the entropy density is only a function of β , and so independent of the degree distribution.

From Eq. (7), we see that the entropy per link diverges at the critical temperature $\beta \rightarrow \beta_c^+ = 1$. This implies that there is a sudden change in the behavior of the system at the critical point $\beta = \beta_c$, which could indicate the presence of a phase transition.

This transition is, however, anomalous –at odds with the continuous entropy density usually observed in continuous phase transitions– and thus cannot be described by Landau’s symmetry-breaking theory of continuous phase transitions. Figure 1 shows a numerical evaluation of the entropy for different system sizes in homogeneous networks confirming the divergence of the entropy per link at the critical temperature as predicted by our analysis. Nevertheless, as we show in Supplementary Note 1.2, entropy per link diverges logarithmically with the system size at $\beta = \beta_c$ so that the divergence can only be detected for very large systems.

Notice that the S^1 model is rotationally invariant both above and below the critical temperature, which implies that there is no symmetry breaking at the critical point. In fact, we argue that β_c separates two distinct phases with different organization of the cycles, or topological defects, in the network. Indeed, the cycle space of an undirected network with N nodes, E links, and N_{com} connected components is a vector space of dimension $E - N + N_{com}$ ³⁷. This dimension is also the number of independent chordless cycles in the network as they form a complete basis of the cycle space. In complex networks, we are typically interested in connected or quasi-connected networks, with a giant connected component extending almost to the entire network. In the S^1 model this is achieved in the percolated phase when the average degree is sufficiently high, but still in the sparse regime so that the vast majority of cycles are contained in the giant component. In this case, by changing temperature without changing the degree distribution, the number of nodes, links, and components remain almost invariant and so does the number of chordless cycles. Thus, the two different phases correspond to a different arrangement of the chordless cycles of the network, as illustrated in the sketch in Fig. 1. This is again similar to the BKT transition since the number of vortices and antivortices is preserved in both phases. We, however, notice that the exact preservation of the number of cycles is not a necessary condition for the transition to take place.

This difference in arrangement of the cycles is caused by the following process. At low temperatures, the high energy associated with connecting spatially distant points causes the majority of links attached to a given node to be local. This defines the geometric phase at $\beta > \beta_c$ where the triangle inequality plays a critical role in the formation of cycles of finite size. As temperature increases, the number of energetically feasible links connecting very distant pairs of nodes grows, and at $\beta \leq \beta_c$ the number of available long-range states becomes macroscopic due to the logarithmic dependence of the energy on distance, which causes the entropy per link to be infinite in this regime. This defines a non-geometric phase where links are mainly long-ranged and the fraction of finite size cycles vanishes because the triangle inequality stops playing a role. This in turn implies that chordless cycles are necessarily of the order of the network diameter.

In the geometric phase, there are finite cycles of any order, although, as we show in Fig. 2, the density of triangles is much higher than the density of squares, pentagons, etc. In the non-geometric phase, the cycles are of the order of the network diameter. However, due to the (ultra) small-world property and finite size effects, the diameter of the network can be quite small, so that the distinction between finite cycles of order higher than three and long-range cycles can be difficult. Therefore, the average local clustering coefficient –measuring the density of the shortest possible cycles, which are also the most numerous– is the perfect order parameter to quantify this topological phase transition.

Finite size scaling behavior of the transition. To quantify the behavior of clustering in this transition, we compute the average local clustering coefficient, \bar{c} , as the local clustering coefficient

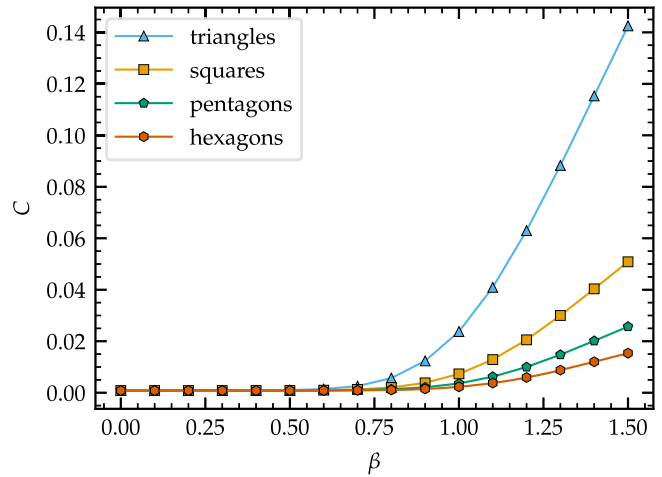


Fig. 2 The global clustering coefficient for different sized chordless cycles as a function of the inverse temperature. The global clustering coefficient is defined as the ratio between the amount of closed n -lets and the total amount of n -lets, where n goes from three (triangles) to six (hexagons). This coefficient is a measure for the amount of different sized chordless cycles, as a function of the inverse temperature β . The results shown are for networks of size $N = 5000$ and $\langle k \rangle = 6$. Error bars representing the standard error are smaller than the data points and therefore not displayed.

averaged over all nodes in a network. The local clustering coefficient for a given node i , with hidden variables (κ_i, θ_i) , is defined as the probability that a pair of randomly chosen neighbors are neighbors themselves and, using results from³⁸, can be computed as

$$c_i = \frac{\sum_{j \neq i} \sum_{k \neq i} P_{ij} P_{jk} P_{ik}}{(\sum_{j \neq i} P_{ij})^2}. \tag{8}$$

In Supplementary Notes 1.3 and 1.4 we derive analytic results for the behavior of the average local clustering coefficient when hidden degrees follow a power law distribution $\rho(\kappa) \sim \kappa^{-\gamma}$ with $2 < \gamma < 3$ and a cutoff $\kappa < \kappa_c \sim N^{\alpha/2}$. Notice that the arguments above, presenting the average local clustering coefficient as an appropriate order parameter, should be valid for all choices of the distribution of the hidden degrees, as long as they lead to sparse graphs. Here, we choose this specific definition because it is the most common in the literature and allows for analytically tractable results. Notice also that it includes both the heterogeneous case with $(\alpha > 1)$ and without $(0 < \alpha \leq 1)$ degree-degree correlations³⁹, as well as the homogeneous case $(\alpha = 0)$, see Supplementary Note 1.3 for the derivation) where $\rho(\kappa) = \delta(\kappa - \langle k \rangle)$.

When $\beta > 1$, i.e. in the geometric region, the average local clustering coefficient behaves as⁹

$$\lim_{N \rightarrow \infty} \bar{c}(N, \beta) = Q(\beta), \tag{9}$$

for some constant $Q(\beta)$ that depends on β . Moreover, there exists a constant Q' such that

$$\lim_{\beta \rightarrow 1^+} \frac{Q(\beta)}{(\beta - 1)^2} = Q'. \tag{10}$$

The analytic results for $\beta \leq 1$ are derived by finding appropriate bounding functions $f(N, \beta) \leq \bar{c}(N, \beta) \leq g(N, \beta)$ that are both asymptotically proportional to $N^{-\sigma(\beta)} h(N, \beta)$, where $h(N, \beta)$ represents some non-power law function of N , implying that $\bar{c} \sim N^{-\sigma(\beta)} h(N, \beta)$ as well. When $\beta' < \beta \leq 1$, i.e. in the quasi-

geometric region,

$$\bar{c}(N, \beta) \sim \begin{cases} (\log N)^{-2} & \text{if } \beta = 1 \\ N^{-2(\beta'-1)} & \text{if } \beta' < \beta < 1 \end{cases} \quad (11)$$

where the value of β' depends on the parameter α . If $\alpha > 1$ it is given by $\beta' = 2/\gamma$ and if κ_c grows with N slower than any power law ($\alpha = 0$) then $\beta' = \frac{2}{3}$. Notice that the behavior in a close neighborhood of β_c is independent of γ . The fact that the microscopic details of the model, in particular the hidden degree distribution, do not affect this scaling behavior points to the universality of our results.

Finally, when $\beta < \beta'$ (in the non-geometric region), the exact scaling behavior depends on α (see the Supplementary Note 1.3 for the case $0 < \alpha \leq 1$):

$$\bar{c}(N, \beta) \sim \begin{cases} N^{-(\gamma-2)} \log N & \text{if } \alpha > 1 \\ N^{-1} & \text{if } \alpha = 0. \end{cases} \quad (12)$$

These results are remarkable in many respects. First, clustering undergoes a continuous transition at $\beta_c = 1$, attaining a finite value in the geometric phase $\beta > \beta_c$ and becoming zero in the non-geometric phase $\beta < \beta_c$ in the thermodynamic limit. The approach to zero when $\beta \rightarrow \beta_c^+$ is very smooth since both clustering and its first derivative are continuous at the critical point. Second, right at the critical point, clustering decays logarithmically with the system size, and it decays as a power of the system size when $\beta < \beta_c$. This is at odds with traditional continuous phase transitions, where one observes a power law decay at the critical point and an even faster decay in the disordered phase. Third, there is a quasi-geometric region $\beta' < \beta < \beta_c$ where clustering decays very slowly, with an exponent that depends on the temperature. Finally, for $\beta < \beta'$, we recover the same result as that of the soft configuration model for scale-free degree distributions³⁴. The results in Eqs. (11) and (12) around the critical point suggest that $N_{\text{eff}} = \ln N$ plays the role of the system size instead of N . Indeed, in terms of this effective size, we observe a power law decay at the critical point and a faster decay in the unclustered phase, as expected for a continuous phase transition. Consequently, we expect the finite size scaling ansatz of standard continuous phase transitions to hold with this effective size. We then propose that, in the neighborhood of the critical point, clustering at finite size N can be written as

$$\bar{c}(\beta, N) = [\ln N]^{-\frac{\eta}{\nu}} f\left(\frac{(\beta - \beta_c)[\ln N]^{\frac{1}{\nu}}}{\nu}\right), \quad (13)$$

with $\eta = 2$, $\nu = 1$, and where $f(x)$ is a scaling function that behaves as $f(x) \sim x^\eta$ for $x \rightarrow \infty$.

We test these results with numerical simulations and by direct numerical integration of Eq. (8) using Eq. (1) for $\beta > \beta_c$ and Eq. (2) for $\beta \leq \beta_c$. Simulations are performed with the degree-preserving geometric (DPG) Metropolis-Hastings algorithm introduced in⁴⁰, that allows us to explore different values of β while preserving exactly the degree sequence. Given a network, the algorithm selects at random a pair of links connecting nodes i, j and l, m and swaps them (avoiding multiple links and self-connections) with a probability given by

$$p_{\text{swap}} = \min \left[1, \left(\frac{\Delta\theta_{ij}\Delta\theta_{lm}}{\Delta\theta_{il}\Delta\theta_{jm}} \right)^\beta \right], \quad (14)$$

where $\Delta\theta$ is the angular separation between the corresponding pair of nodes. This algorithm maximizes the likelihood that the network is \mathbb{S}^1 geometric while preserving the degree sequence and the set of angular coordinates, and it does so independently of whether the system is above or below the critical temperature.

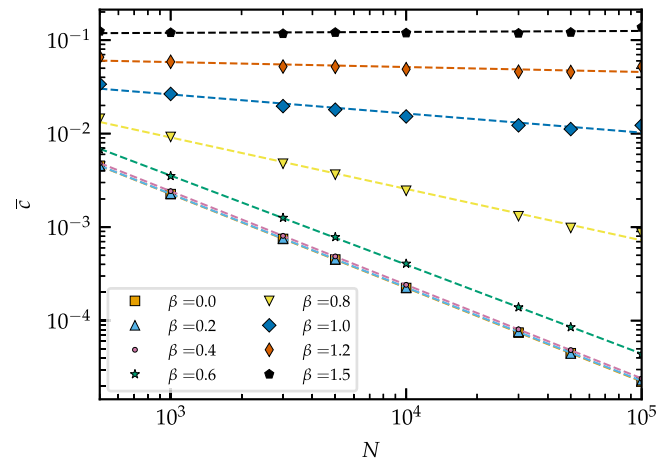


Fig. 3 The average local clustering coefficient as a function of the network size. The networks were generated by applying the DPG technique to a configuration model network with a homogeneous degree sequence $k = 4, \forall k$. Dashed lines are power law fits used to estimate the exponent $\sigma(\beta)$ defined as $\bar{c} \sim N^{-\sigma(\beta)}$. Errorbars representing the standard error are smaller than the data points and therefore not displayed.

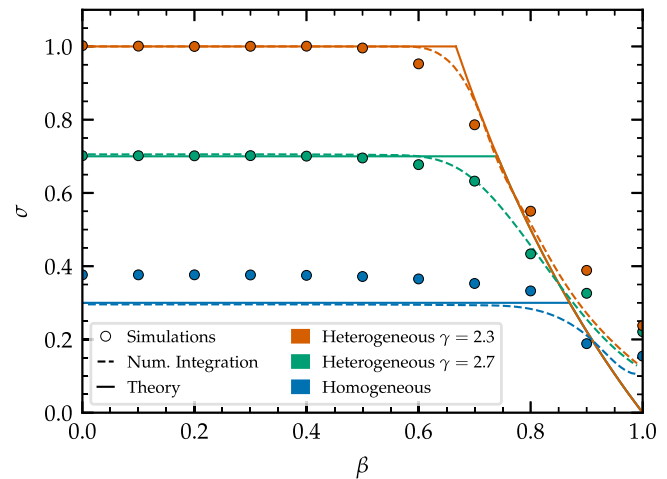


Fig. 4 Exponent of the average local clustering coefficient as a function of the inverse temperature. The exponent $\sigma(\beta)$, defined by $\bar{c}(N, \beta) \sim N^{-\sigma(\beta)} h(N, \beta)$, with $h(N, \beta)$ a non-power law function of N , evaluated from numerical simulations (colored circles), numerical integration of Eq. (8) (dashed lines), and theoretical approach Eqs. (11) and (12) (solid lines). Networks are generated with a homogeneous distribution of hidden degrees (red lines and circles) and a power law distribution with exponents $\gamma = 2.3$ and $\gamma = 2.7$, blue and green lines and circles, respectively. Errorbars representing the standard error are smaller than the data points and therefore not displayed.

Notice that the continuity of Eq. (14) as a function of β makes it evident that, even if the connection probability takes a different functional form above and below the critical point, the model is the same.

Figure 3 shows the behavior of the average local clustering coefficient as a function of the number of nodes for homogeneous \mathbb{S}^1 networks with different values of β , showing a clear power law dependence $N^{-\sigma(\beta)}$ in the non-geometric phase $\beta < \beta_c$, with an exponent that varies with β as predicted by our analysis. These results are used to measure the exponent $\sigma(\beta)$ as a function of the inverse temperature β , which in Fig. 4 are compared with the theoretical value given by Eqs. (11) and (12). The agreement is in general very good, although it gets worse for values of β very close

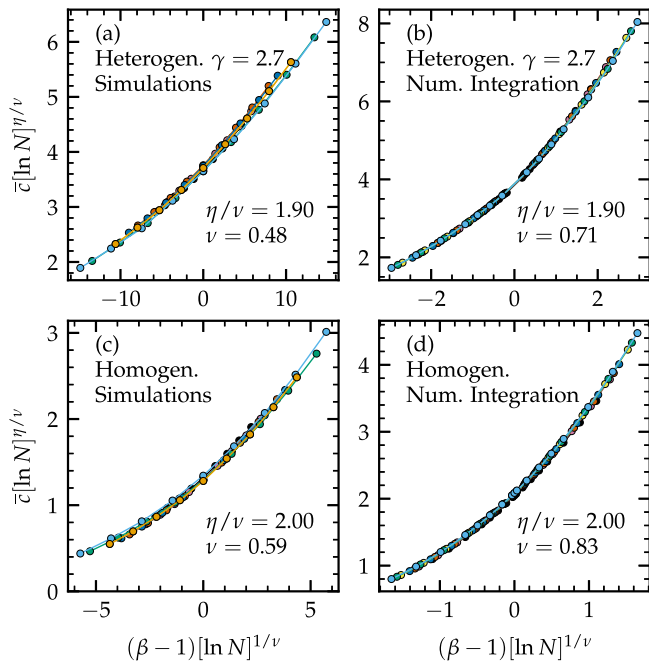


Fig. 5 Finite size scaling analysis. Data collapse of the average local clustering coefficient at different sizes as defined in Eq. (13) for heterogeneous networks with $\gamma = 2.7$ (panels (a) and (b)) and homogeneous networks (panels (c), and (d)). The panels (a) and (c) correspond to numerical simulations with sizes in the range $N \in (5 \times 10^2, 10^5)$, whereas the panels (b) and (d) are obtained from numerical integration of Eq. (8) with sizes in the range $N \in (5 \times 10^5, 10^8)$. Different colors correspond to the different system sizes used. Error bars representing the standard error are smaller than the data points and therefore not displayed.

to β_c and for very heterogeneous networks. This discrepancy is expected due to the slow approach to the thermodynamic limit in the non-geometric phase, which suggests that the range of our numerical simulations, $N \in [5 \times 10^2, 10^5]$, is too limited. To test for this possibility, we solve numerically Eq. (8) for sizes in the range $N \in [5 \times 10^5, 10^8]$ and measure numerically the exponent $\sigma(\beta)$. In this case, the agreement is also very good for heterogeneous networks. The remaining discrepancy when $\beta \approx \beta_c$ is again expected since, as shown in Eq. (11), right at the critical point clustering decays logarithmically rather than as a power law. Finally, Fig. 5 shows the finite size scaling Eq. (13) both for the numerical simulations and numerical integration of Eq. (8). In both cases, we find a very good collapse with exponent $\eta/\nu \approx 2$ in all cases. The exponent ν , however, departs from the theoretical value $\nu = 1$ in numerical simulations due to their small sizes but improves significantly with numerical integration for bigger sizes. We then expect Eq. (13) to hold, albeit for very large system sizes.

The slow decay of clustering in the non-geometric phase implies that some real networks with significant levels of clustering may be better described using the \mathbb{S}^1 model with temperatures in the quasi-geometric regime $\beta < \beta_c$. Given a real network, the DPG algorithm can be used to find its value of β . To do so, nodes in the real network are given random angular coordinates in $(0, 2\pi)$. Then the DPG algorithm is applied, increasing progressively the value of β until the average local clustering coefficient of the randomized network matches the one measured in the real network. Many real networks have very high levels of clustering and lead to values of $\beta > \beta_c$. However, there are

notable cases with values of β below the critical point. As an example, in Supplementary Note 2 we show values of β obtained for several real networks with values below or slightly above β_c . In fact, some of them are found to be very close to the critical point, like protein-protein interaction networks of specific human tissues⁴¹, with $\beta \approx 1$, or the genetic interaction network of the *Drosophila Melanogaster*⁴², $\beta \approx 1.1$.

Conclusions

The \mathbb{S}^1 model shows different behavior of the average local clustering coefficient on the left and right side of $\beta_c = 1$. To understand if there is a phase transition that goes beyond clustering, we cast the model into a framework of Fermi statistics and compute the entropy of the ensemble. The result shows that the entropy diverges at the critical point, implying a change in the structural organization of the system as a whole. Because the model is rotational invariant in both regimes, one can conclude that this transition is not due to symmetry breaking. The behavior of clustering—non-zero on the right and vanishing on the left of the critical point—indicates that the transition is of topological nature related to the organization of cordless cycles. As the model around the critical point is in the small-world regime, the largest cycles are, at most, of the order $\ln N$ on both sides. This implies that short cycles, like triangles, are more appropriate as the order parameter to study the phase transition.

As the \mathbb{S}^1 model is geometric in nature, the set of states that edges—considered noninteracting particles in the Fermi description—can occupy are correlated by the triangle inequality in the underlying metric space. This correlation induces an effective interaction between particles, ultimately leading to a clustered phase at low temperatures and to the anomalous phase transition described above. Interestingly, the logarithmic dependence of the state-energy with the metric distance results in the divergence of the entropy at a finite temperature β_c and, thus, to a different ordering of cycles below β_c , where clustering vanishes in the thermodynamic limit. The finite size behavior of the transition is anomalous, with $\ln N$ and not N playing the role of the system size. This slow approach to the thermodynamic limit is relevant for real networks in the quasi-geometric phase $\beta' < \beta < 1$, for which high levels of clustering can still be observed. All together, our results describe an anomalous topological phase transition that cannot be described by the classic Landau theory but that, nevertheless, differs from other topological phase transitions, such as the BKT transition, in the behavior of thermodynamic properties.

Data availability

The data that support the findings of this study is available from the corresponding authors on request.

Code availability

The custom computer code that support the findings of this study is available from the corresponding authors on request.

Received: 23 November 2021; Accepted: 21 September 2022;

Published online: 06 October 2022

References

1. Hohenberg, P. C. & Krekhov, A. P. An introduction to the Ginzburg–Landau theory of phase transitions and nonequilibrium patterns. *Phys. Rep.* **572**, 1–42 (2015).

2. Berezinskii, V. Destruction of long-range order in one-dimensional and two-dimensional systems having a continuous symmetry group. I. Classical systems. *Sov. Phys. JETP*. **32**, 493–500 (1971).
3. Berezinskii, V. Destruction of long-range order in one-dimensional and two-dimensional systems possessing a continuous symmetry group. II. Quantum systems. *Sov. Phys. JETP*. **34**, 610–616 (1972).
4. Kosterlitz, J. M. & Thouless, D. J. Ordering, metastability and phase transitions in two-dimensional systems. *J. Phys. C: Solid State Phys.* **6**, 1181–1203 (1973).
5. Mermin, N. D. & Wagner, H. Absence of Ferromagnetism or Antiferromagnetism in One- or Two-Dimensional Isotropic Heisenberg Models. *Phys. Rev. Lett.* **17**, 1133–1136 (1966).
6. Chiu, C.-K., Teo, J. C. Y., Schnyder, A. P. & Ryu, S. Classification of topological quantum matter with symmetries. *Rev. Mod. Phys.* **88**, 035005 (2016).
7. Boguñá, M. et al. Network geometry. *Nat. Rev. Phys.* **3**, 114–135 (2021).
8. Boguñá, M., Krioukov, D., Almagro, P. & Serrano, M. Á. Small worlds and clustering in spatial networks. *Phys. Rev. Res.* **2**, 023040 (2020).
9. Serrano, M. Á., Krioukov, D. & Boguñá, M. Self-Similarity of Complex Networks and Hidden Metric Spaces. *Phys. Rev. Lett.* **100**, 078701 (2008).
10. Bringmann, K., Keusch, R. & Lengler, J. Geometric inhomogeneous random graphs. *Theor. Comput. Sci.* **760**, 35–54 (2019).
11. Kosmidis, K., Havlin, S. & Bunde, A. Structural properties of spatially embedded networks. *EPL* **82**, 48005 (2008).
12. Biskup, M. On the scaling of the chemical distance in long-range percolation models. *Ann. Probab.* **32**, 2938–2977 (2004).
13. Millán, A. P., Gori, G., Battiston, F., Enns, T. & Defenu, N. Complex networks with tuneable spectral dimension as a universality playground. *Phys. Rev. Res.* **3**, 023015 (2021).
14. Krioukov, D., Papadopoulos, F., Kitsak, M., Vahdat, A. & Boguñá, M. Hyperbolic geometry of complex networks. *Phys. Rev. E*. **82**, 036106 (2010).
15. Gugelmann, L., Panagiotou, K. & Peter, U. Random Hyperbolic Graphs: Degree Sequence and Clustering. In *Autom Lang Program (ICALP 2012, Part II)*, LNCS 7392 (2012).
16. Candellero, E. & Fountoulakis, N. Clustering and the Hyperbolic Geometry of Complex Networks. *Internet Math.* **12**, 2–53 (2016).
17. Fountoulakis, N., van der Hoorn, P., Müller, T. & Schepers, M. Clustering in a hyperbolic model of complex networks. *EJP* **26**, 1–132 (2021).
18. Abdullah, M. A., Fountoulakis, N. & Bode, M. Typical distances in a geometric model for complex networks. *Internet Math.* **1** (2017).
19. Friedrich, T. & Krohmer, A. On the Diameter of Hyperbolic Random Graphs. *SIAM J. Discrete Math.* **32**, 1314–1334 (2018).
20. Müller, T. & Staps, M. The diameter of KPKVB random graphs. *Adv. Appl. Probab.* **51**, 358–377 (2019).
21. Serrano, M. Á., Krioukov, D. & Boguñá, M. Percolation in Self-Similar Networks. *Phys. Rev. Lett.* **106**, 048701 (2011).
22. Fountoulakis, N. & Müller, T. Law of large numbers for the largest component in a hyperbolic model of complex networks. *Ann. Appl. Probab.* **28**, 607–650 (2018).
23. Kiwi, M. & Mitsche, D. Spectral gap of random hyperbolic graphs and related parameters. *Ann. Appl. Probab.* **28**, 941–989 (2018).
24. Papadopoulos, F., Kitsak, M., Serrano, M. Á., Boguñá, M. & Krioukov, D. Popularity versus similarity in growing networks. *Nature* **489**, 537–540 (2012).
25. Allard, A., Serrano, M. Á., García-Pérez, G. & Boguñá, M. The geometric nature of weights in real complex networks. *Nat. Commun.* **8**, 14103 (2017).
26. Kleineberg, K.-K., Boguñá, M., Serrano, M. Á. & Papadopoulos, F. Hidden geometric correlations in real multiplex networks. *Nat. Phys.* **12**, 1076–1081 (2016).
27. Kleineberg, K.-K., Buzna, L., Papadopoulos, F., Boguñá, M. & Serrano, M. Á. Geometric Correlations Mitigate the Extreme Vulnerability of Multiplex Networks against Targeted Attacks. *Phys. Rev. Lett.* **118**, 218301 (2017).
28. Zuev, K., Boguñá, M., Bianconi, G. & Krioukov, D. Emergence of Soft Communities from Geometric Preferential Attachment. *Sci. Rep.* **5**, 9421 (2015).
29. García-Pérez, G., Serrano, M. Á. & Boguñá, M. Soft Communities in Similarity Space. *J. Stat. Phys.* **173**, 775–782 (2018).
30. Muscoloni, A. & Cannistraci, C. V. A nonuniform popularity-similarity optimization (nPSO) model to efficiently generate realistic complex networks with communities. *New. J. Phys.* **20**, 052002 (2018).
31. García-Pérez, G., Boguñá, M. & Serrano, M. Á. Multiscale unfolding of real networks by geometric renormalization. *Nat. Phys.* **14**, 583–589 (2018).
32. Zheng, M., García-Pérez, G., Boguñá, M. & Serrano, M. Á. Scaling up real networks by geometric branching growth. In *Proc. of the National Academy of Sciences* **118**, e2018994118 (2021).
33. Park, J. & Newman, M. E. J. Statistical Mechanics of Networks. *Phys. Rev. E*. **70**, 66117 (2004).
34. Colomer-de Simón, P. & Boguñá, M. Clustering of random scale-free networks. *Phys. Rev. E*. **86**, 026120 (2012).
35. van der Hoorn, P., Lippner, G. & Krioukov, D. Sparse maximum-entropy random graphs with a given power-law degree distribution. *J. Stat. Phys.* **173**, 806–844 (2018).
36. Garlaschelli, D., den Hollander, F. & Roccaverde, A. Covariance structure behind breaking of ensemble equivalence in random graphs. *J. Stat. Phys.* **173**, 644–662 (2018).
37. Gross, J. L., Yellen, J. & Anderson, M. Graph theory and its applications (Chapman and Hall/CRC, 2018).
38. Boguñá, M. & Pastor-Satorras, R. Class of Correlated Random Networks with Hidden Variables. *Phys. Rev. E* **68**, 36112 (2003).
39. Boguñá, M., Pastor-Satorras, R. & Vespignani, A. Cut-offs and finite size effects in scale-free networks. *Eur. Phys. J. B Condens. Matter* **38**, 205–209 (2004).
40. Starnini, M., Ortiz, E. & Serrano, M. Á. Geometric randomization of real networks with prescribed degree sequence. *New J. Phys.* **21**, 053039 (2019).
41. Chang, A. et al. BRENDA in 2015: exciting developments in its 25th year of existence. *Nucl. Acids Res.* **43**, D439–D446 (2014).
42. Stark, C. et al. BioGRID: a general repository for interaction datasets. *Nucl. Acids Res.* **34**, D535–D539 (2006).

Acknowledgements

We acknowledge support from Agencia estatal de investigación project number PID2019-106290GB-C22/AEI/10.13039/501100011033 and Generalitat de Catalunya grant number 2017SGR1064. M. B. acknowledges the ICREA Academia award, funded by the Generalitat de Catalunya. J. vd K. acknowledges support from the Secretaria d'Universitats i Recerca de la Generalitat de Catalunya i del Fons Social Europeu.

Author contributions

J. vd K. did the calculations and numerical simulations. M.A.S. participated in the design and implementation of the research and supervised the work. M.B. did some of the analytical calculations, participated in the design and implementation of the research and supervised the work. All authors discussed the results and implications and wrote the manuscript.

Competing interests

The authors declare no competing interests.

Additional information

Supplementary information The online version contains supplementary material available at <https://doi.org/10.1038/s42005-022-01023-w>.

Correspondence and requests for materials should be addressed to Marián Boguñá.

Peer review information *Communications Physics* thanks Pim van der Hoorn and the other, anonymous, reviewer(s) for their contribution to the peer review of this work. Peer reviewer reports are available.

Reprints and permission information is available at <http://www.nature.com/reprints>

Publisher's note Springer Nature remains neutral with regard to jurisdictional claims in published maps and institutional affiliations.



Open Access This article is licensed under a Creative Commons Attribution 4.0 International License, which permits use, sharing, adaptation, distribution and reproduction in any medium or format, as long as you give appropriate credit to the original author(s) and the source, provide a link to the Creative Commons license, and indicate if changes were made. The images or other third party material in this article are included in the article's Creative Commons license, unless indicated otherwise in a credit line to the material. If material is not included in the article's Creative Commons license and your intended use is not permitted by statutory regulation or exceeds the permitted use, you will need to obtain permission directly from the copyright holder. To view a copy of this license, visit <http://creativecommons.org/licenses/by/4.0/>.

© The Author(s) 2022